A Novel Structure Type in Reduced Rare-Earth Metal Halides. One-Dimensional Confacial Chains Based on Centered Square Antiprismatic Metal Units: Y_4Br_4Os and Er_4Br_4Os

Peter K. Dorhout[†] and John D. Corbett*

Contribution from the Department of Chemistry, Iowa State University, Ames, Iowa 50011.
Received July 18, 1991

Abstract: The isostructural title compounds are synthesized from dendritic Y or Er (R), sublimed RBr_3, and Os in welded Nb containers at 850–1020 °C. The crystal structure of Y_4Br_4Os has been established by single-crystal X-ray means ($C2/c$, $Z = 8$; $a = 12.514$ (5) Å, $b = 12.381$ (4) Å, $c = 6.567$ (2) Å, $\beta = 90.96$ (3)°; R, $R_w(F) = 3.5$, 3.9%). The structure consists of osmium-centered antiprisms that share opposed square faces to generate quasi-infinite chains, viz., $Y_{8/2}(Os)Br_4$. Successive shared faces are tilted in opposite directions by ~±4°, and the bromine atoms are displaced from coplanar positions in the direction of the tilt so as to cap four adjoining metal triangles on the shorter side of each antiprismatic unit. A fourth, comparable interchain Y–Br^{a-i} bond is also formed by every Y and Br atom. The face-sharing square antiprismatic building blocks, the face capping of triangular cluster faces by halogen, and the intimate interchain bridging are all new for centered cluster halides. The need for distortion to gain the interchain bonding, the advantages of face capping of centered antiprismatic polyhedra, and the different behavior of the isoelectronic Ta_4Te_4Si are considered. Y_4Br_4Os exhibits a small Pauli-like paramagnetism.

Introduction

Historically, explorations for metal-rich halides of the rare-earth elements have revealed a variety of diverse compounds and structure types. Several recent reviews have addressed the growing number and complexity of these new materials and the characterization of their physical properties.[1,2] Recently, our group has explored the stabilization of rare-earth metal (R) iodide cluster phases by the novel encapsulation of certain transition-metal atoms Z within the clusters. These efforts have yielded compounds $R_6I_{10}Z$[3] and $R_7I_{12}Z$[4,5] that contain discrete clusters as well as those in which clusters have been formally condensed into chain or network structures, namely for R_4I_5Z[6] and for two versions with the stoichiometry R_3I_3Z.[7,8] Octahedral (trigonal antiprismatic) metal units R_6 centered by Z are the basic building blocks throughout.

It has become evident during these investigations that the products obtained are often subtly dependent on the sizes and nature of both the host metal R and the halogens. Reduced yttrium chlorides, for example, show only a sparse interstitial chemistry.[9] It is also well-known that reduced yttrium halides often exhibit compositions and structures that are very similar to those of the heavier and smaller lanthanide elements, Gd and beyond.[1,2,10-14] Both effects appear important in the present study in which we discovered a novel structure type R_4Br_4Os for R = Y and Er, one of several new phases in a family of condensed yttrium and erbium bromides that are stabilized by encapsulated transition metals. The new R_4Br_4Os structure is based on confacial square antiprismatic R_8 units, but the chain proportions and the robust interchain bridging by sheathing bromine distinguish it from the kindred Ta_4Te_4Si recently reported by Badding and DiSalvo.[15]

Experimental Section

Syntheses. The origin and purity of the elemental starting materials, the high-temperature synthetic methods, and the Guinier powder X-ray diffraction methods have all been described before.[3-5] The reactants in the form of crushed dendritic rare-earth metal (Ames Lab), sublimed RBr_3 previously prepared from the metal and NH_4Br,[16] and osmium (Johnson Matthey) were welded in niobium tubes. Substantially quantitative yields of the desired phases were observed in stoichiometric reactions run at 900 °C for 30 days. Beautiful black, well-faceted needles as long as 0.5 mm that were suitable for single-crystal X-ray diffraction were grown out of a NaBr flux in a reaction that was heated from 850 to 950 °C over 24 h, held at 950 °C for 12 days, and slowly cooled at 5 °C/h to 800 °C. The compounds are very sensitive to moisture and perhaps oxygen and decompose rapidly into a brown syrup upon exposure to air. Lattice constants for both Y_4Br_4Os and Er_4Br_4Os based on indexed Guinier patterns are given in Table I.

Unlike previous studies involving condensed iodides, we saw no evidence for any competing phase at lower temperatures (850 °C) where

Table I. Lattice Parameters (Å, deg) of R_4Br_4Os Phases (Space Group $C2/c$)[a]

	Y_4Br_4Os	Er_4Br_4Os
a	12.514 (5)	12.434 (5)
b	12.381 (4)	12.321 (3)
c	6.567 (2)	6.492 (1)
β	90.96 (3)	90.92 (3)

[a] Refined from Guinier powder diffraction patterns with Si as an internal standard; $\lambda = 1.54056$ Å.

Table II. Some Crystal and Refinement Data for Y_4Br_4Os

space group, Z	$C2/c$ (No. 15), 8
V,[a] Å^3	1017.4 (7)
μ(Mo Kα), cm^{-1}	504.3
transmissn coeff range	0.34–1.00
no. obsd data, $F_o^2 > 3\sigma(F_o^2)$	654
no. parameters	42
R, %	3.5
R_w, %	3.9

[a] Lattice dimensions in Table I. [b] $R = \sum||F_o| - |F_c||/\sum|F_o|$. [c] $R_w = [\sum w(|F_o| - |F_c|)^2/\sum w(F_o)^2]^{1/2}$; $w = [\sigma(F)]^{-2}$.

[†] Current address: Department of Chemistry, Colorado State University, Fort Collins, CO 80523.

(1) (a) Meyer, G. *Prog. Sol. State Chem.* **1982**, *14*, 141. (b) Meyer, G. *Chem. Rev.* **1988**, *88*, 93.
(2) Simon, A. *Angew. Chem., Int. Ed. Engl.* **1988**, *27*, 159.
(3) Hughbanks, T.; Corbett, J. D. *Inorg. Chem.* **1988**, *27*, 2022.
(4) Hughbanks, T.; Corbett, J. D. *Inorg. Chem.* **1989**, *28*, 631.
(5) Payne, M. W.; Corbett, J. D. *Inorg. Chem.* **1990**, *29*, 2246.
(6) Payne, M. W.; Dorhout, P. K.; Corbett, J. D. *Inorg. Chem.* **1991**, *30*, 1467.
(7) Dorhout, P. K.; Payne, M. W.; Corbett, J. D. *Inorg. Chem.*, in press.
(8) Payne, M. W.; Dorhout, P. K.; Kim, S.-J.; Hughbanks, T. R.; Corbett, J. D. *Inorg. Chem.*, submitted for publication.
(9) Meyer, H.-J.; Corbett, J. D. Unpublished research.
(10) Mattausch, Hj.; Hendricks, J. B.; Egar, R.; Corbett, J. D.; Simon, A. *Inorg. Chem.* **1980**, *19*, 2128.
(11) Berroth, K.; Mattausch, Hj.; Simon, A. *Z. Naturforsch.* **1980**, *B35*, 626.
(12) Meyer, G.; Hwu, S.-J.; Wijeyesekera, S.; Corbett, J. D. *Inorg. Chem.* **1986**, *25*, 4811.
(13) Kauzlarich, S. M.; Hughbanks, T.; Corbett, J. D.; Klavins, P.; Shelton, R. N. *Inorg. Chem.* **1988**, *27*, 1791.
(14) Nagaki, D.; Simon, A.; Borrmann, H. *J. Less-Common Met.* **1989**, *156*, 193.
(15) Badding, M. E.; DiSalvo, F. J. *Inorg. Chem.* **1990**, *29*, 3952.
(16) Meyer, G.; Dötsch, S.; Staffel, T. *J. Less-Common Met.* **1987**, *127*, 155.

0002-7863/92/1514-1697$03.00/0

Table III. Positional and Isotropic Equivalent Thermal Parameters for Y_4Br_4Os

atom	x	y	z	B_{eq},[a] Å^2
Y1	0.0762 (2)	0.1772 (1)	−0.0097 (3)	0.77 (7)
Y2	0.1759 (2)	−0.0760 (1)	0.0097 (3)	0.84 (7)
Br1	−0.1197 (2)	0.3048 (1)	−0.0989 (3)	1.36 (8)
Br2	0.3073 (2)	0.1130 (1)	−0.1000 (3)	1.38 (8)
Os	0	0.00570 (8)	1/4	0.54 (4)

[a] $B_{eq} = (8\pi^2/3)\sum_i\sum_j U_{ij}a_i^*a_j^*\vec{a}_i\vec{a}_j$.

Table IV. Important Bond Distances (Å) and Angles (deg) in Y_4Br_4Os

Distances			
Os–Os	3.287 (1) (2×)	Y1–Br1	2.966 (3)
Os–Y1	2.895 (2) (2×)		3.074 (3)
	2.911 (2) (2×)	Y1–Br2	3.068 (3)
Os–Y2	2.896 (2) (2×)		3.059 (3)[c]
	2.912 (2) (2×)	Y2–Br1	2.979 (3)
Y1–Y1[a]	3.935 (4)		3.048 (3)[c]
	3.660 (4)	Y2–Br2	2.957 (3)
Y1–Y2[a]	3.823 (3)		3.057 (3)
	3.636 (3)	Br1–Br2[d]	3.549 (3)
Y2–Y2[a]	3.785 (2)		3.564 (3)
Y1–Y2[b]	3.376 (3)	Os–Br1[e]	4.249 (2)
	3.394 (3)	Os–Br2[e]	4.219 (3)
Angles			
Os–Os–Os	175.08 (6)	Os–Y1–Br2[c]	159.81 (9)
Y1–Y2–Y1	89.97 (6)	Os–Y2–Br1[c]	160.07 (8)
Y2–Y1–Y2	90.03 (6)	Y1–Br2–Y2[c]	151.61 (8)
Y1–Br1–Y2[c]	154.91 (9)	Y1–Br2–Y2[c]	124.91 (7)
Y2–Br1–Y1[c]	127.28 (9)	Y1–Br2–Y1[c]	100.48 (7)
Y1–Br1–Y2[e]	102.26 (8)	Y1–Br2–Y2[e]	68.14 (7)
Y1–Br1–Y2[e]	69.62 (6)	Y1–Br2–Y2[e]	72.84 (7)
Y1–Br1–Y2[e]	73.82 (6)	Y2–Br2–Y2[e]	77.00 (7)
Y1–Br1–Y1[e]	74.56 (8)		

[a] In triangular face. [b] In square face. [c] Interchain function. [d] d(Br–Br) < 3.6 Å. [e] Within face-capping function.

we have usually obtained $R_6I_{10}Z$ and $R_7I_{12}Z$ cluster phases.[5,6,8] Temperatures as high as 1020 °C also yielded only R_4Br_4Os. It was common to find ~5% ROBr as a contaminant from adventitious oxygen.

Structural Study. Diffraction data from a small needle crystal of Y_4Br_4Os were collected at 23 °C on a Rigaku AFC6R diffractometer using monochromated Mo Kα radiation and a 12-kW rotating anode generator. Previous Weissenberg photographic studies of the $hk0$ and $hk1$ nets had established a C-centering monoclinic cell with a probable space group $C2/c$ based on systematic absences in hkl ($h + k \neq 2n$) and $h0l$: ($h, l \neq 2n$). Cell constants and an orientation matrix obtained from a least-squares refinement of 20 centered reflections found during the automated search routine on the diffractometer appeared to corroborate the C-centered monoclinic cell.

A full hemisphere of data was collected out to $2\theta \leq 50.1°$ with no restrictions and with ω–2θ scans at 16.0°/min in ω; weak reflections ($I/\sigma_I < 10$) were rescanned up to twice. R_{ave} was 8.7% for all data. Absorption was corrected empirically with the aid of the average of three ψ scans.

The structure was solved using direct methods (SHELXS[17]) which provided positions for all five independent atoms. The least-squares refinement proceeded uneventfully and converged at R, $R_w(F) = 3.5$, 3.9%. The final difference Fourier map showed maximum and minimum peaks of 2.4 and −2.3 e$^-$/Å^3, respectively, the former being 2.42 Å from Br2. Selected crystal and refinement data for Y_4Br_4Os are in Table II, and atomic positions and isotropic equivalent thermal parameters for Y_4Br_4Os can be found in Table III.

Magnetic Susceptibilities. Data were collected on a Quantum Design MPMS SQUID magnetometer at a field of 3.0 T over the range 6–300 K with measurements at 10 K intervals. Quantitative samples (30–40 mg) were sealed between two fused silica rods (3-mm o.d.) inside a fused silica tube (3-mm i.d.) and under <1 atm of He. The data were corrected for core diamagnetism with 2.0×10^{-4} emu/mol of R_4I_4Os.

Results and Discussion

Unlike condensed iodide phases, these R_4I_4Os products with R = Y or Er can be prepared in high yields over a wide temperature range (850–975 °C) from a range of stoichiometries, probably because there appear to be no competing phases. Moreover, we have so far found these products only when they incorporate osmium. Similar stoichiometries and reaction conditions yield either no reaction (Z = Fe, Ag, Au) or other new phases (Z = Si, Mn, Re, Ru, Ir, Pt) that are not isotypic. No other lanthanide host elements (R) have been tried to date.

The structure of Y_4Br_4Os (Er_4Br_4Os) can best be described in terms of osmium-centered square antiprisms of yttrium (erbium) condensed into chains by sharing square faces, as illustrated in Figure 1. A list of important distances and angles in the yttrium version is given in Table IV. The shared centrosymmetric faces are nearly perfect squares with 90° angles within 0.5σ and Y–Y

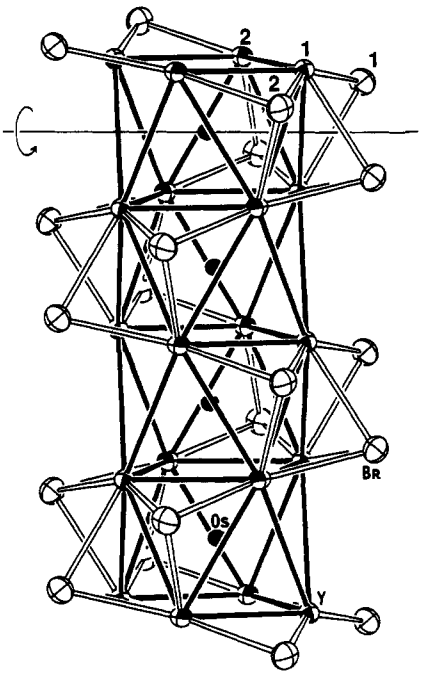

Figure 1. Approximate [$\bar{1}$00] view of a portion of one chain of Y_4Br_4Os (two cells) illustrating the "clam shell" nature of the distorted square antiprisms. Yttrium atoms are octant shaded, osmium atoms are solid, and bromine atoms are crossed (90% probability thermal) ellipsoids. (The shared squares are centrosymmetric, and 2-fold axes bisect the Y1–Y1 edges of each antiprism, as marked for the top cluster.)

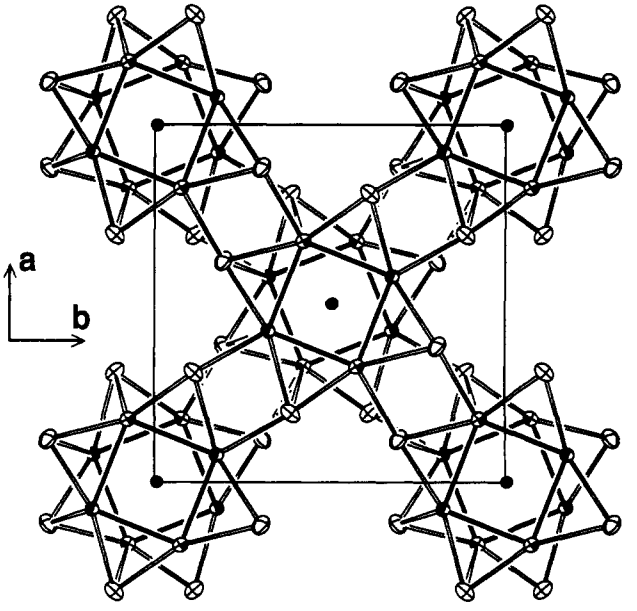

Figure 2. [001] section of Y_4Br_4Os showing interchain bridging. 2-Fold axes lie along 0, y, $^1/_4$ and $^1/_2$, y, $^1/_4$. The atom designations are the same as in Figure 1.

(17) Sheldrick, G. M. SHELXS-86, Institut für Anorganische Chemie, Universität Göttingen, Germany.

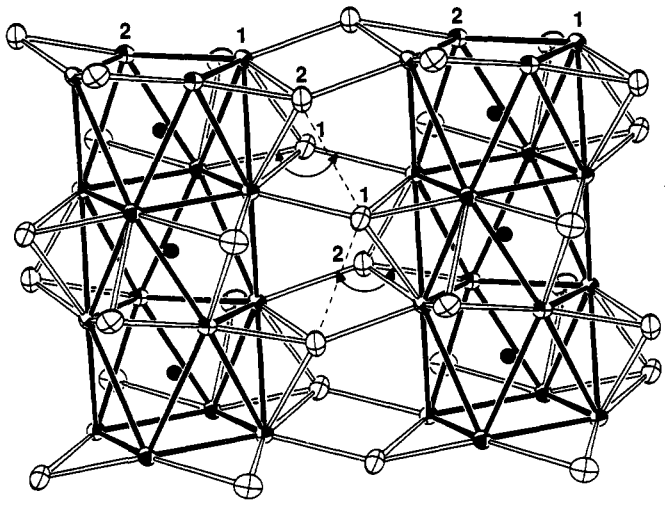

Figure 3. [$\bar{1}$10] view of two chains showing the interchain bridging by bromine atoms. Independent pairs of the largest intercluster Y–Br–Y bond angles and the shortest Br···Br separations are marked (see text).

edges of 3.375 (3) and 3.394 (3) Å. Successive faces along the chain have staggered stacking (43.9° offset) but are not parallel (dihedral angle 172.3 (1)°). This means that triangular faces about the waists of the antiprisms have a range of sizes, the extremes alternating from one side of the chain to the other. A projection of the C-centered arrangement of the chains along $\vec{c}$ is shown in Figure 2, where 2-fold axes parallel to $\vec{b}$ lie at x = 0, $^1/_2$. The shortest interchain Y–Y distance is 4.693 Å.

Bromine atoms sheath the metal chains as well as bridge between them. Based on other halide structures, a reasonable arrangement a priori would be for the four bromine atoms to be three-bonded, bridging each of the four edges of the shared metal squares and also being bonded exo, but probably more distantly, to yttrium vertices in other chains. However, the sizes of all three elements in the present compound seem particularly favorable as they allow some distortions and an increase to four in the number of Y–Br bonds for each atom. Not only do the triangular side faces of the metal chain have different sizes, as noted above, but the Y–Y edges running between the shared squares are also 0.26–0.55 Å longer than within, presumably because of the relative size of Os (below). Successive squares in each column tilt in alternate directions, and all bromine atoms are further displaced ~15° out of these planes in concert with their tilting. The four smaller neighboring triangles about the waist of each antiprism are thereby systematically capped with bromine, as shown in Figure 1. Conversely, four more exposed yttrium vertices about the more open edge of each antiprism from which the bromines have moved away are now able to bond to face-capping bromine atoms on the closed sides of antiprisms in four neighboring chains, as shown in Figures 2 and 3. In the Schäfer–Schnering nomenclature,[18] the structure can be described simply as $Y_{8/2}$-(Os)Br^{i-a}_4 since bromine is not shared between adjoining antiprisms. (The Br^{i-a} notation denotes an inner capping (or bridging) atom functionality Br^i that is also outer (exo or ausser) to other chains.)

The resulting arrangement can be likened to a chain of confacial "clams", hinged at the smaller triangles and with open edges that face in alternate directions along the chain. The osmium "pearl" lies on a 2-fold axis along 0, y, $^1/_4$ that threads through each "clam" on the open edge and hinge, specifically bisecting the short and long Y1–Y1 edges (see Figure 1). These distortions, which presumably have only a small cost in the electronic energy of the Y–Y and Y–Os bonding, must have a considerable benefit as far as the gain from additional Y–Br bonding. Two Y_3 triangles adjoin each shared Y–Y edge in the square antiprismatic chains, and the systematic displacement of bromine up or down to cover *half* of these triangles provides increased Y–Br bonding within the chain *and* room to generate strong interchain bridges as well (below). The polarity of the Y–Br bonds is doubtlessly important in the stability of all such structures.

The distortions observed appear necessary since comparable but idealized square antiprismatic chains constructed of coplanar yttrium and bromine atoms would probably not allow strong interchain $Y–Br^{a-i}$ bonding owing to steric hindrance from the neighboring bromines on the second chain. Such a model allows only 3.5-Å interchain Y···Br "bonds", 0.45 Å greater than observed, if Br^i···Br^a closed-shell contact limits of 3.6 Å are imposed. In fact, cluster and condensed cluster halides usually exhibit intercluster bridge distances $M–X^a$ that are appreciably longer than the $M–X^i$ separations, particularly for the larger halides or smaller interstitials,[19] and many of these differences appear to be the direct result of similar X^i···X^a contact repulsions. The remarkably smaller differences between $Y–Br^i$ and $Y–Br^a$ distances achieved in Y_4Br_4Os testify to the effectiveness of the distortions, which afford 2.967–3.068 Å for the former vs 3.048 and 3.059 Å for $Y–Br^a$. The outward pointing "frontier" orbitals at the metal vertices that are responsible for bridging between these confacial square antiprismatic bromide chains are obviously strongly bonding relative to those available with confacial *trigonal* antiprismatic units in $^1_\infty[MoS_3^-]$, for example.[20] Non-metal bonding to metal along the chains is distinctly different, however, because of chain proportions (below).

The foregoing accommodations still leave clear distortions in the interchain bridging (Table IV). Interchain angles Y1–Br–Y2 of over 150° are present (Figure 3), and the $Os–Y–Br^a$ angles are 20° less than the 180° ideal. The need for these distortions can be traced to the presence of Br···Br contacts of 3.55–3.56 Å in the interchain galleries, one set of which is dashed in Figure 3. These distances appear quite short relative to the smallest closed-shell contacts in other bromides, 3.68 Å in $Sc_7Br_{12}C$,[21] 3.82 Å in Gd_2Br_2C,[22] and 3.77 Å in $ErBrH_{0.7}$,[12] and they approach even that found with a higher field cation in ZrBr, 3.50 Å.[23]

The Y–Y bond lengths in Y_4Br_4Os average 3.635 Å and are comparable to those in other systems, 3.710–3.928 Å in $Y_6I_{10}Os$[5] and 3.266–3.694 Å in Y_2Cl_3.[10] However, the polyhedral dimensions in the two centered examples are probably determined largely by Os–Y bonding distances which average 2.903 Å in Y_4Br_4Os with eight contacts vs the smaller 2.704 Å in $Y_6I_{10}Os$ with six. Such simple comparisons of course neglect both electronic effects in the two different cluster polyhedra and their different states of aggregation, although it is at least novel that the two formally have the same electron counts per cavity. Clearly, the halogen to metal proportion has primary control over the degree of condensation.

A noteworthy aspect of this cluster structure is that the halide atoms cap *faces* on the metal cluster. This is relatively rare and heretofore limited largely to binary examples. The older are octahedral clusters of relatively small metals, $Mo_6X_8^{4+}(X^-)_4$ and $Nb_6I_8^{3+}(I^-)_3$ (and its hydride), where the last listed halides in each have only intercluster bridging roles, but face-capping halide is also found in molybdenum and rhenium chalcogenide halides.[24] It has been supposed[25] that there is insufficient room for 12 edge-bridging halides on these, although their electron-rich character is probably also a factor favoring 8-fold sheathing. Other examples of face-capping halide on metal octahedra occur in the rare and unique Gd_2Cl_3-type chain structure known for R = Y, Gd, and Tb with X = Cl and Br,[10,26] in the double-chain phase Sc_7Cl_{10},[27] and in the double-metal-layered ZrCl and ZrBr.[23,28]

(18) Schäfer, H.; Schnering, H.-G. *Angew. Chem.* **1964**, *76*, 833.
(19) Ziebarth, R. P.; Corbett, J. D. *J. Am. Chem. Soc.* **1989**, *111*, 3272.
(20) Hughbanks, T.; Hoffmann, R. *J. Am. Chem. Soc.* **1983**, *105*, 1150.
(21) Dudis, D. S.; Corbett, J. D.; Hwu, S.-J. *Inorg. Chem.* **1986**, *25*, 3434.
(22) Schwanitz-Schüller, U.; Simon, A. *Z. Naturforsch.* **1985**, *406*, 710.
(23) Daake, R. L.; Corbett, J. D. *Inorg. Chem.* **1977**, *16*, 2029.
(24) (a) Perrin, C.; Chevrel, R.; Sergent, M.; Fischer, Ø. *Mat. Res. Bull.* **1979**, *14*, 1505. (b) Perrin, C.; Potel, M.; Sergent, M. *Acta Crystallogr.* **1983**, *C39*, 415. (c) Perrin, A.; Leduc, L.; Sergent, M. *Eur. J. Solid State Inorg. Chem.* **1991**, *28*, 919.
(25) Corbett, J. D. *J. Solid State Chem.* **1981**, *37*, 343.
(26) (a) Lokken, D. A.; Corbett, J. D. *Inorg. Chem.* **1973**, *12*, 556. (b) Simon, A.; Holzer, N.; Mattausch, Hj. *Z. Anorg. Allg. Chem.* **1979**, *456*, 207.

All of the many other cluster, condensed cluster, and sheet structures constructed from groups III and IV transition metals and halide evidently require interstitial elements, and these exhibit only edge-bridged M_6X_{12} type clusters or their fragments (other than for centered hydride in $Nb_6I_{11}(H)$[29]). It has been noted[30] that one factor mitigating against a face capping of a centered octahedral cluster is that this configuration brings the capping halide and the interstitial too close to one another, particularly when the latter is a non-metal. The idealized arrangement IA

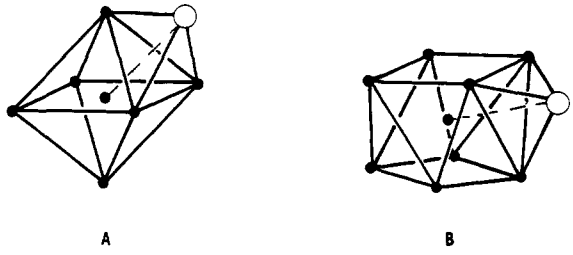

I

for a $Y_6(Os)Br_8$ octahedron with d(Y–Os) = 2.7 Å (as in $Y_6I_{10}Os$) and d(Y–Br) = 3.0 Å produces a Br···Os separation of 3.6 Å for face capping vs 4.2 Å for edge-bridging bromine. The idealized face-capped square antiprism IB with d(Y–Os) = 2.9 Å affords a distinctly longer Br···Os separation of 4.1 Å, which is 0.5 Å greater than for the ideal octahedron. (The observed structure gives even greater separations, 4.22 and 4.25 Å.) This scenario also allows somewhat closer yttrium–yttrium contacts which presumably act as a stabilizing force for the square antiprism since chain HOMO's are mainly Y–Y, etc., bonding.[6,8,13] Obviously, all of the factors discussed above influence the stability of this structure, although further subtle features must contribute to and account for the general preponderance of centered octahedral fragments. The dominant role played by alternate phases in determining stability, or not, remains.

The contrast between Y_4Br_4Os and the isoelectronic Ta_4Te_4Si[15] is striking because the latter contains chains of fairly undistorted confacial antiprisms in which the edges of shared square faces are simply bridged by coplanar tellurium. Crystals of the telluride naturally are relatively fragile since there is no direct interchain bonding and the chains are held together by only van der Waals forces. The origin of the differences between the two chain structures can be explained in largely dimensional terms, both in the proportions of the antiprisms and in the relative halogen–chalcogen sizes. It is difficult to correlate the cluster dimensions with a single set of standard metallic radii since the latter usually utilize only the tetrahedral covalent value for silicon. However, the fact of the matter is that the antiprismatic clusters in Ta_4Te_4Si are appreciably flattened compared with those in Y_4Br_4Os. The average Si–Ta and Os–Y distances are 2.593 and 2.903 Å, respectively, while the edges of the square faces are much more similar, 3.250 Å (Ta) and 3.384 Å (Y). This means the smaller silicon produces an antiprismatic "sandwich" that is more compressed along the chain, so that the average Ta–Ta edge length about the antiprism waist is nearly 0.8 Å less than the analogous Y–Y separations in Y_4Br_4Os. (Direct Si–Si bonding may also play a role.[31]) Accordingly, the ratios of lengths of the independent metal–metal edges in these two antiprismatic examples differ by 21%.

The chain compression in Ta_4Te_4Si and the marginally larger size of tellurium both have the effect of inhibiting intercluster bridging. As with the idealized Y_4Br_4Os discussed earlier, the tantalum vertices are withdrawn from the centers of the approximate squares of nearest-neighbor tellurium atoms in Ta_4Te_4Si (d(Te···Te) = 3.84–3.89 Å). This means a potential exo Te^a from another chain can realize a Ta–Te distance no shorter than 3.45 Å when limited by 3.6-Å Te^i···Te^a van der Waals contacts with those in the surrounding square. Such interchain bridging seems improbable in comparison with regular Ta–Te distances within the chain, which are 0.53–0.62 Å less. Distortion of the relatively taller antiprisms in Y_4Br_4Os is also favored by somewhat smaller bromine and, doubtlessly, by the additional and stronger Y–Br bonds that are achieved therewith.

Other analogues of Ta_4Te_4Si have also been identified by powder diffraction means with Al, Cr, Fe, Co, or Ni as alternate interstitials[15] as well as a comparable series with niobium chains.[32] These will probably contain similar or somewhat smaller clusters based on the relative Si–Al–Fe size effects established within isolated $Zr_6I_{14}Z$-type clusters.[33]

There are, of course, other structures containing confacial chains of centered square antiprisms, but in none are the chains so well isolated as those in Y_4Br_4Os and Ta_4Te_4Si. The W_5Si_3 type is perhaps the most similar, containing confacial square antiprismatic chains of tungsten centered by silicon.[34] These are relatively flattened and interconnected by common edge-bridging silicon atoms such that comparable interchain W–W distances develop. There is also a second linear chain of tungsten in the structure within probable bonding distances of the first. Phases like Pr_5Sn_3, $Zr_5(Al,Ga,Ge,Si)_3$, and $(Ta,Nb)_5(Si,Ge)_3$ occur in this structure.[35] The ultimate degree of condensation in which the bridging anions (Br, Te) have been eliminated is found in the structure of $CuAl_2$.[36]

Magnetic Data. Magnetic susceptibility data for Er_4Br_4Os follow the Curie–Weiss law over the entire temperature range with a Weiss constant of −8 K (Figure 4, supplementary material). The fit yields a moment of 16.6 μ_B for Er_4Br_4Os or 8.3 μ_B per Er atom. This result is somewhat lower than would be expected for the free ion $4f^{11}$ configuration of Er^{3+}, 9.59 μ_B.[37] Spin–orbital coupling in this unusual osmium "complex" is apt to be responsible,[4] although other possible coupling mechanisms in such structures are not at all well understood. The yttrium analogue with its diamagnetic cores displays a very small paramagnetic signal that slowly increases with decreasing temperature, e.g., 4.3, 5.0, and 6.0×10^{-4} emu/mol at 3 T and 296, 125, and 55 K, respectively (after core correction). This suggests a Pauli paramagnetism and a metallic conductor.

Conductivity measurements have not been attempted on single crystals of either phase owing to their small size and high sensitivity to moisture. Deduction of conductivity (and bonding) expectations for Y_4Br_4Os on the basis of predictions for the related Ta_4Te_4Si secured by extended-Hückel means[31] is complicated particularly by the change in antiprism proportions, the different bonding orbitals available on the interstitials, and the character of the non-metal bonding. Nonetheless, the centered polyhedral bonding does appear to dominate many features of the bonding in such cases, and the breadth of the conduction band calculated for Ta_4Te_4Si encourages us to predict a similar metallic character for Y_4Br_4Os and Er_4Br_4Os. The magnetic data for the former increase our boldness. The isoelectronic relationship between the two diverse examples of antiprismatic chains is particularly novel, since the valence electron contributions of all three component elements are different. Notwithstanding, this similarity does not contribute any understanding to the formation of alternate Y_xBr_yZ phases for the neighboring Z = Ru, Rh, and Ir, however. We

(27) Poeppelmeier, K. R.; Corbett, J. D. *Inorg. Chem.* **1977**, *16*, 1107.
(28) Adolphson, D. G.; Corbett, J. D. *Inorg. Chem.* **1976**, *15*, 1820.
(29) Simon, A. *Z. Anorg. Allg. Chem.* **1967**, *355*, 295.
(30) Hwu, S.-J.; Corbett, J. D.; Poeppelmeier, K. R. *J. Solid State Chem.* **1985**, *57*, 43.
(31) Li, J.; Hoffmann, R.; Badding, M. E.; DiSalvo, F. J. *Inorg. Chem.* **1990**, *29*, 3943.
(32) Ziebarth, R. P.; Badding, M.; DiSalvo, F. J. Unpublished research, cited in ref 15.
(33) Hughbanks, T.; Rosenthal, G.; Corbett, J. D. *J. Am. Chem. Soc.* **1988**, *110*, 1511.
(34) Aronsson, D. *Acta Chem. Scand.* **1955**, *9*, 1107.
(35) Villars, P.; Calvert, L. D. *Pearson's Handbook of Crystallographic Data for Intermetallic Phases*; America Society of Metals: Metals Park, OH, 1991; Vol. 1, p 395.
(36) Hyde, B. G.; Andersson, S. *Inorganic Crystal Structures*; Wiley: New York, 1989; p 291.
(37) Kittel, C. *Introduction to Solid State Physics*, 6th ed.; Wiley: New York, 1986; p 405.

are presently studying analogous lanthanide iodide phases containing both 3d and 5d interstitials that also contain antiprismatic chains.

Acknowledgment. The magnetic data were obtained through the cooperation of J. E. Ostenson. This research was supported by the National Science Foundation, Solid State Chemistry, via Grant DMR-8902954 and was carried out in facilities of the Ames Laboratory, DOE.

Supplementary Material Available: Tables of crystal and refinement data and of anisotropic atom displacement parameters for Y_4I_4Os and the Curie–Weiss plot of the susceptibility of Er_4Br_4Os (Figure 4) (3 pages); a table of observed and calculated structure factor data for Y_4I_4Os (5 pages). Ordering information is given on any current masthead page.

Models of Heme d_1. Molecular Structure and NMR Characterization of an Iron(III) Dioxoisobacteriochlorin (Porphyrindione)

K. M. Barkigia,*[1a] C. K. Chang,[1b] J. Fajer,[1a] and M. W. Renner*[1a]

Contribution from the Department of Applied Science, Brookhaven National Laboratory, Upton, New York 11973, and Department of Chemistry, Michigan State University, East Lansing, Michigan 48824. *Received August 8, 1991*

Abstract: Crystallographic and NMR results are reported for **4**, the $ClFe^{III}$ complex of 2,7-dioxo-3,3′,8,8′,12,13,17,18-octaethylporphyrin (**3**). **4** serves as a model for heme d_1, the unusual dioxoisobacteriochlorin (iBC = isobacteriochlorin) prosthetic group of bacterial dissimilatory nitrite reductases. The coordination and displacement of the Fe in **4** are similar to those found in pentacoordinate, high-spin iron(III) porphyrins, as is the domed conformation of its macrocycle. The major differences are the distinct elongation of the Fe–N distances to the saturated pyrroline rings, 2.118 (6) and 2.113 (6) Å, vs those to the pyrrole rings, 2.047 (6) and 2.033 (6) Å. The shorter Cα–Cβ pyrroline bonds bearing the keto groups vs those without the oxygens suggest that the keto groups are in conjugation with the macrocycle π system. These structural data thus provide a rationale for the most distinctive feature between iBCs and dioxo-iBCs: the large differences in Fe and macrocycle redox potentials. In contrast to the influence of the keto groups on the redox and pyrroline structural properties of **4**, NMR data, particularly at the meso positions, are comparable to those recently reported for $ClFe^{III}$OEiBC (Sullivan et al. *J. Am. Chem. Soc.* **1991**, *113*, 5264). Iterative extended Hückel calculations for the HOMOs and LUMOs of **4** correctly predict the effects of the keto groups on the redox properties of the macrocycle. Crystallographic results for the free base **3**, although at poorer precision than for **4**, indicate that the NH protons are localized on adjacent pyrrole rings and that the macrocycle is not inherently ruffled to any significant extent. Crystallographic data for **4**: space group $P\bar{1}$, $a = 11.635$ (3) Å, $b = 16.189$ (5) Å, $c = 9.003$ (5) Å, $\alpha = 96.93$ (3)°, $\beta = 95.92$ (3)°, $\gamma = 93.75$ (2)°, $V = 1669.2$ Å^3, $Z = 2$. The structure was refined against 2421 data points with $F_o > 2\sigma F_o$ to $R_F = 0.065$ and $R_{wF} = 0.064$.

Introduction

The crucial roles of chlorophylls and bacteriochlorophylls in light harvesting and energy conversion in photosynthesis have long focused attention on the physical, chemical, and structural properties of these chromophores.[2] However, an increasing body of evidence indicates that the generic class of hydroporphyrins, porphyrins in which one or more β–β pyrrole bonds are saturated, mediates a wide range of biological functions in addition to photosynthetic reactions. Among the "green" hemes that catalyze biological reactions as diverse as assimilatory and dissimilatory nitrite reductions,[3,4] sulfite reductions,[3] and catalase activity,[5,6] is heme d_1, the iron isobacteriochlorin (iBC)[7] prosthetic group of bacterial dissimilatory nitrite reductases. Heme d_1 is deduced to consist of an unusual dioxoisobacteriochlorin[7] (**1**).

Two salient features of hydroporphyrins have emerged from recent theoretical, experimental, and structural studies of chlorins, bacteriochlorins, and isobacteriochlorins. First, saturation of one or more β–β pyrrole bonds of porphyrins causes shifts of the lowest unoccupied (LUMOs) and highest occupied (HOMOs) molecular orbitals[8] with the results that reduction and oxidation potentials as well as optical spectra are altered.[8-10] Second, the increased saturation of the hydroporphyrins renders them more flexible,[11-15]

(1) (a) Brookhaven National Laboratory. (b) Michigan State University.
(2) For examples, see: *Chlorophylls*, Scheer, H., Ed.; CRC Press, Boca Raton, FL, 1991. *Reaction Centers of Photosynthetic Bacteria*; Michel-Beyerle, M. E., Ed.; Springer-Verlag: Berlin, 1990.
(3) Siegel, L. M.; Murphy, M. J.; Kamin, H. *J. Biol. Chem.* **1973**, *248*, 251. Murphy, M. J.; Siegel, L. M.; Kamin, H. *Ibid.* **1973**, *248*, 2801. Murphy, M. J.; Siegel, L. M.; Tove, S. R.; Kamin, H. *Proc. Natl. Acad. Sci. U.S.A.* **1974**, *74*, 6121. Vega, J. M.; Garret, R. H. *J. Biol. Chem.* **1975**, *250*, 7980. Ostrowski, J.; Wu, J. Y.; Rueger, D. C.; Miller, B. E.; Siegel, L. M.; Kredich, N. M. *J. Biol. Chem.* **1989**, *264*, 15726.
(4) Horie, S.; Watanabe, T.; Nakamura, S. *J. Biochem.* **1976**, *80*, 579. Kim, C. H.; Hollocher, T. C. *J. Biol. Chem.* **1983**, *258*, 4861.
(5) Jacob, G. S.; Orme-Johnson, W. H. *J. Biol. Chem.* **1979**, *18*, 2967.
(6) Chiu, J. T.; Loewen, P. C.; Switala, J.; Gennis, R. B.; Timkovich, R. *J. Am. Chem. Soc.* **1989**, *111*, 7046.
(7) Chang, C. K.; Timkovitch, R.; Wu, W. *Biochemistry* **1986**, *25*, 8447. Wu, W.; Chang, C. K. *J. Am. Chem. Soc.* **1987**, *109*, 3149. Chang, C. K.; Wu, W. *J. Biol. Chem.* **1986**, *261*, 8593. Weeg-Aerssens, E.; Wu, W.; Ye, R. W.; Tiedje, J. M.; Chang, C. K. *J. Biol. Chem.* **1991**, *266*, 7496.
(8) Chang, C. K.; Hanson, L. K.; Richardson, P. F.; Young, R.; Fajer, J. *Proc. Natl. Acad. Sci. U.S.A.* **1981**, *78*, 2652.
(9) Stolzenberg, A. M.; Spreer, L. O.; Holm, R. H. *J. Am. Chem. Soc.* **1980**, *102*, 364. Stolzenberg, A. M.; Strauss, S. H.; Holm, R. H. *J. Am. Chem. Soc.* **1981**, *103*, 4763.
(10) Richardson, P. F.; Chang, C. K.; Hanson, L. K.; Spaulding, L. D.; Fajer, J. *J. Phys. Chem.* **1979**, *83*, 3420. Richardson, P. F.; Chang, C. K.; Spaulding, L. D.; Fajer, J. *J. Am. Chem. Soc.* **1979**, *101*, 7736. Chang, C. K.; Fajer, J. *J. Am. Chem. Soc.* **1980**, *102*, 848. Fujita, E.; Chang, C. K.; Fajer, J. *J. Am. Chem. Soc.* **1985**, *107*, 7665.
(11) Eschenmoser, A. *Ann. N.Y. Acad. Sci.* **1986**, *471*, 108. Kratky, C.; Waditschatka, R.; Angst, C.; Johansen, J. E.; Plaquevent, J. C.; Schreiberg, J.; Eschenmoser, A. *Helv. Chim. Acta* **1985**, *68*, 1312 and references therein.

0002-7863/92/1514-1701$03.00/0